Micro-tensile strength of a welded turbine disc superalloy

Oluwasegun, Kunle; Cooper, C.; Chiu, Yu-Lung; Jones, I.p.; Li, Hangyue; Baxter, G.

DOI:
10.1016/j.msea.2013.12.046

Document Version
Publisher's PDF, also known as Version of record

Citation for published version (Harvard):
Oluwasegun, K, Cooper, C, Chiu, Y-L, Jones, IP, Li, H & Baxter, G 2014, 'Micro-tensile strength of a welded turbine disc superalloy', *Materials Science and Engineering A*, vol. 596, pp. 229-235. https://doi.org/10.1016/j.msea.2013.12.046

Materials Science & Engineering A 596 (2014) 229–235

Contents lists available at ScienceDirect

Materials Science & Engineering A

journal homepage: www.elsevier.com/locate/msea

Rapid communication

Micro-tensile strength of a welded turbine disc superalloy

K.M. Oluwasegun [a], C. Cooper [a], Y.L. Chiu [a], I.P. Jones [a], H.Y. Li [a,*], G. Baxter [b]

[a] School of Metallurgy and Materials, University of Birmingham, B15 2TT, United Kingdom
[b] Rolls-Royce plc., P.O. Box 31, Derby DE24 8BJ, United Kingdom

ARTICLE INFO

Article history:
Received 26 October 2013
Received in revised form
13 December 2013
Accepted 15 December 2013
Available online 21 December 2013

Keywords:
Small-scale testing
Superalloys
Friction welding

ABSTRACT

A micro-tensile testing system coupled with focussed ion beam (FIB) machining was used to characterise the micro-mechanical properties of the weld from a turbine disc alloy. The strength variations between the weld and the base alloy are rationalised via the microstructure obtained.

1. Introduction

The development of micro-scale experiments has been initiated by the need to evaluate the mechanical behaviour of small volumes of materials and also by a desire to determine how the mechanical properties of a material change when external dimensions are greatly reduced [1–5]. Micro-tensile testing has been effectively used to characterise the mechanical properties of thin films, e.g. of MEMS.

The methods often used in preparing micro-tensile specimens include material deposition on substrate (additive process) [6–8], deep reactive ion etching (subtractive process) [9] and electro-discharge machining [10]. All these methods have been successfully used, but cannot be adopted for applications where a particular site of interest within a large volume of material is needed to be characterised. Focussed ion beam (FIB) is an invaluable tool for fabricating micron-sized structures, due to its ability to deposit Pt or W in controlled shapes, the availability of submicron (20–50 nm) ion beams, 3-D stages, and fully automated control [11].

Aside from the high accuracy in local positioning through direct visual control, in situ micro-tensile testing also offers insight into the real time material deformation process.

Micro-tensile tests have been carried out to characterise the local properties within fusion welds of HY-100 steel [10,12] and of two dissimilar stainless steels [13]. The strength at the centre of the weld was found to be considerably higher than that away from the centre. However, the dimensions of these microsamples ($300 \times 200 \times 200\ \mu m^3$) are larger than many welds produced by solid state techniques. For instance, inertia friction welding often produces much narrower welds with a bond line zone about 50 μm wide compared with the 1300 μm of typical fusion welds. Solid state joining is increasingly used in the aeroengine industry for multicomponent turbine engines. Detailed material characterisation within the narrow weld zone, where microstructural variation from the parent material has occurred, is essential to understand the overall mechanical performance of welded joints. The hardness of an inertia friction welded (IFW) RR1000 superalloy has been reported to be higher than that of the parent material [14]. As a result the true yield stress of the weld zone cannot be measured by standard tensile testing procedures [15].

This paper reports in-situ micro-tensile deformation of IFW RR1000, focussing on the yielding.

2. Materials and methods

RR1000 is a recently developed (Rolls Royce) nickel base superalloy processed via powder metallurgy with a nominal chemical composition of (wt%) 15.0 Cr, 18.5 Co, 5.0 Mo, 3.0 Al, 3.6 Ti, 2.0 Ta, 0.5 Hf, 0.015 B, 0.06 Zr, 0.027 C and balance nickel.

A thin cross-section slice was extracted from an inertia welded tube in RR1000 by electro-discharge machining (EDM). It was ground and thinned before a wedge shaped sample, which contained both the parent and the weld regions, was cut out (Fig. 1). The wedge shaped sample was further ground and polished to a thickness of about 100 μm. Micro-tensile samples with a 13 μm gauge length and 2 μm by 3 μm cross section were prepared from the wedge shape sample using a Quanta 3D FEG SEM FIB with a Ga^+ ion source operated at 30 kV.

* Corresponding author. Tel.: +44 121 4142 880; fax: +44 121 414 7468.
E-mail address: h.y.li.1@bham.ac.uk (H.Y. Li).

0921-5093/$ - see front matter © 2013 Elsevier B.V. All rights reserved.
http://dx.doi.org/10.1016/j.msea.2013.12.046

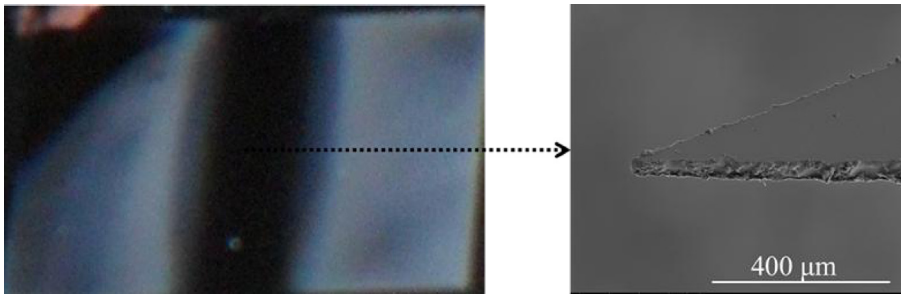

Fig. 1. A wedge shaped specimen (taken from the dark/etched (weld region) of the sample (mounted in conductive bakelite)) used in FIB for micro-tensile sample preparation.

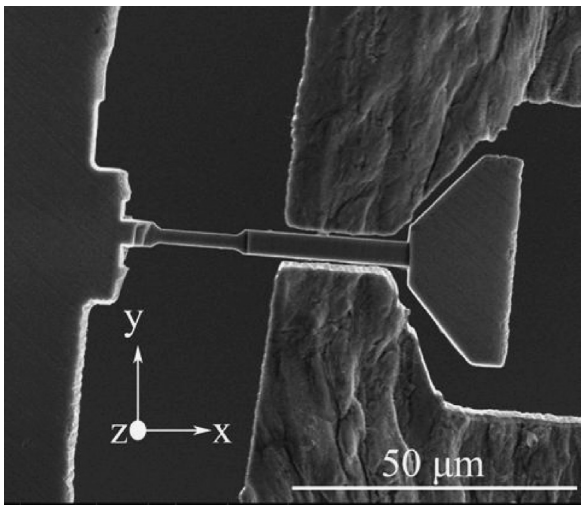

Fig. 2. SEM picture of a micro-tensile sample ($13 \times 2 \times 3\ \mu m^3$) prepared from the base alloy (Parent 1) and fitted into the sample grip before loading.

The microtesting system used in this study includes a piezo-electric drive to apply the load to the sample via a miniature load cell with a load capacity of 0.5 N and a resolution of 0.001 mN. The tensile system was under displacement control at a resolution of 40 nm. The applied load and elongation were measured, and used to plot a stress–strain curve, together with the recorded SEM images.

Electron back scatter diffraction (EBSD) was employed to determine the loading direction and the active slip systems, in order to evaluate the critical resolved shear stresses.

3. Results and discussion

Fig. 2 shows a micro-tensile specimen prepared from the parent RR1000. This specimen was tested by pulling to fracture. Fig. 3b is the stress vs. strain plot obtained from the tensile test. From both the in-situ observation of the formation of slip and the stress–strain results of this test, the yield strength of the alloy and the ultimate tensile strength were determined to be 619 MPa and 699 MPa, respectively.

The sample loading direction [$\bar{2}00$] was determined using the EBSD Kikuchi pattern from the grain in the sample gauge length as illustrated in Fig. 3d. The slip plane was determined to be ($\bar{1}11$) from the orientation relationship between the slip band on the sample and the Kikuchi pattern (plane trace analysis). Since slip direction is on slip plane, $(hkl)\,[uvw]=0$ was used to determine the corresponding slip direction [$\bar{1}10$]. Although more than one direction can satisfy this condition and since it is also difficult to determine the actual slip plane and direction by using only the EBSD Kikuchi pattern, the slip system that gives the highest Schmid's factor has been selected for the plastic deformation of the sample. The selected plane was validated by measuring the angle between the slip band and a plane on the Kikuchi pattern. Table 1 shows the schmid factors calculated for the twelve easy slip systems in the crystal structure. Critical resolved shear stress, τ_c calculated for the sample of about 253 MPa can be estimated via the Schmid equation.

Another tensile sample prepared from the parent material with loading direction [$\bar{5}30$] was tested, and the sample was observed to start yielding at a stress level of 530 MPa by the activation of the ($\bar{1}11$) [$\bar{1}0\bar{1}$] slip system. A τ_c of 255 MPa can be derived, which agrees well with the value obtained for the previous sample.

Fig. 4 shows a micro-tensile sample prepared from the bond line of the weld with loading direction [$3\bar{6}1$]. It was observed that the sample yielded at a stress level of 604 MPa (Fig. 4b and c) via the activation of two slip systems ($1\bar{1}1$)[$01\bar{1}$] and ($1\bar{1}1$)[011] (Fig. 4e) and a critical resolved shear stress of 300 MPa can be estimated.

Another sample prepared from the bond line zone with a [$13\bar{3}$] loading direction was also tested. This sample yielded at 713 MPa on ($1\bar{1}1$)[110] with a critical resolved shear stress of 306 MPa (Table 2). This consistency in the critical resolved shear stress measured indicates that micro-tensile testing is viable for testing local strength.

Another sample was prepared from the weld zone where constitutional liquation features were observed on the grain boundaries (Fig. 5a). EBSD shows that the grain boundary between grains A and B, and that between B and C, are typical high angle grain boundaries. It was observed that the sample started yielding in grain A, the slip bands then propagated into grains B and C, and the sample subsequently failed along the liquated grain boundary between B and C (Fig. 5h). This suggests that the high angle boundary, where a significant constitutional liquation product was observed, was weakened. Table 2 shows a summary of the tensile data from the experiment.

It is generally expected that the yield strength within the weld of a γ′ strengthened nickel base alloy should be greater than in the base alloy. This is because the re-precipitation of a high volume fraction of tertiary γ′ in the size range 10–40 nm at the weld increases the strength [14,16]. The size and distribution of γ′ of the weld and the parent are compared in Fig. 6.

It is evident from Table 2 that the critical resolved shear stress in the weld is indeed higher than that in the base alloy. Although there is a slight uncertainty in the alignment of the length axis of the sample and of the sample holder in the z direction, efforts were made to ensure that the flanks of the sample holder and of the sample head are parallel and equally spaced in order to minimise out-of-plane loading of the specimens, as illustrated in Fig. 2. The measured yield strength in the micro-tensile samples is lower (~30%) than the expected yield strength in the bulk material. This could be a result of the size with crystallographic orientation of the micro-tensile sample [17–19].

Based on the premise that the deformation of γ′ precipitation hardened nickel alloys at room temperature is via two coupled

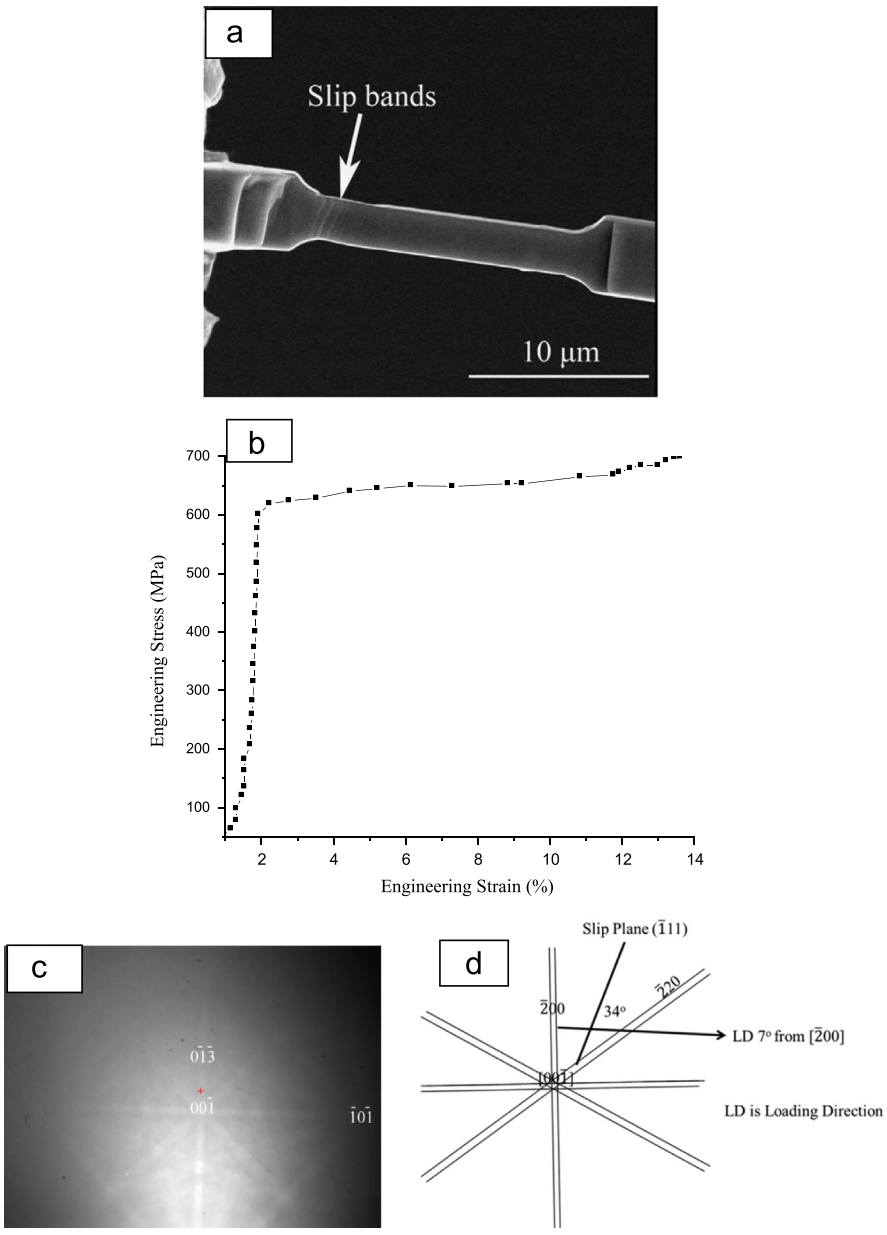

Fig. 3. Micro-tensile sample (a) at 10.8% strain, (b) stress–strain curve of the micro-tensile and (c) EBSD Kikuchi pattern from the specimen with single crystal (foil normal 7° from $00\bar{1}$). *Note*: All EBSD Kikuchi patterns in this work are analysed with the beam direction pointing downwards↓. (d) schematic diagram illustrating the orientation relationship between Kikuchi patterns, sample loading direction and slip.

Table 1
FCC slip system identification.

Index	Slip plane	Slip direction	Schmid factor for $[\bar{2}00]$ stress axis	Schmid factor for $[\bar{5}30]$ stress axis	Schmid factor for $[3\bar{6}\bar{1}]$ stress axis	Schmid factor for$[13\bar{3}]$ stress axis
1	$(11\bar{1})$	[011]	0	−0.0720	0.1243	0
2	$(11\bar{1})$	[101]	0.4082	0.1200	0.0355	0.3008
3	$(11\bar{1})$	$[1\bar{1}0]$	0.4082	0.1921	0.1598	0.3008
4	$(1\bar{1}\bar{1})$	$[01\bar{1}]$	0	0.2882	0.4438	0.1289
5	**$(1\bar{1}\bar{1})$**	**[101]**	0.4082	**0.4803**	0.1775	0.0430
6	**$(1\bar{1}\bar{1})$**	**[110]**	**0.4082**	0.1921	0.2663	0.0859
7	**$(1\bar{1}1)$**	**[011]**	0	0.2882	**0.4970**	0
8	$(1\bar{1}1)$	$[10\bar{1}]$	0.4082	0.4803	0.2840	0.4297
9	**$(1\bar{1}1)$**	**[110]**	0.4082	0.1921	0.2130	**0.4297**
10	(111)	$[01\bar{1}]$	0	0.0720	0.1775	0.1289
11	(111)	$[10\bar{1}]$	0.4082	0.1201	0.1420	0.0859
12	(111)	$[1\bar{1}0]$	0.4082	0.1921	0.3195	0.0430

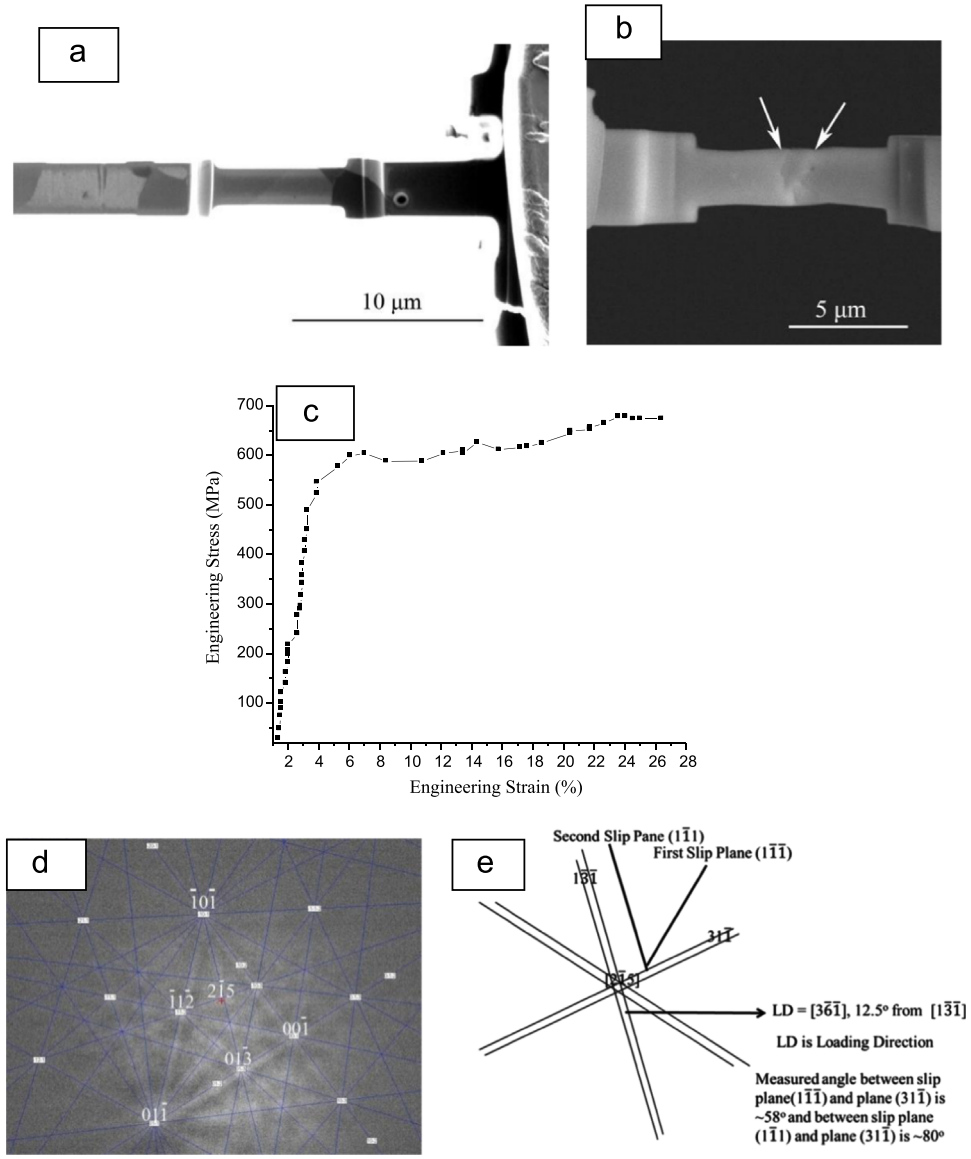

Fig. 4. Micro-tensile sample (6.4 μm × 1.8 μm × 2.2 μm) from BLZ of weld (1) showing (a and b) microstructures at various strain levels, illustrating the initiation of slip steps, (c) stress–strain curve of the micro-tensile specimen prepared from the weld, (d) EBSD Kikuchi pattern from the grain within the sample gauge length and (e) schematic diagram illustrating the orientation relationship between Kikuchi patterns, sample loading direction, and slip planes.

Table 2
A summary of data from the micro-tensile test (at room temperature) of the parent and as-welded RR1000 superalloy.

Region	Parent (1)	Parent (2)	Weld (1)	Weld (2)
Yield strength, (σ_y), MPa	619.03	530.21	603.68	712.50
Loading direction	[$\bar{2}$00]	[$\bar{5}$30]	[3$\bar{6}\bar{1}$]	[13$\bar{3}$]
Slip system	($\bar{1}$11)[1$\bar{1}$0]	($\bar{1}$11)[$\bar{1}$0$\bar{1}$]	(1$\bar{1}$1)[011]	(1$\bar{1}$1)[110]
Schmid factor	0.4082	0.4803	0.4970	0.4297
Critical resolved shear stress (τ_c), MPa	253	255	300	306

edge dislocation moving in the ⟨110⟩ direction on the {111} plane, for small tertiary γ′, according to Brown and Ham [20] and Huther and Rappich [21] the CRSS can be estimated as the stress necessary to move weakly coupled dislocation pairs through the γ′ precipitate, and is given as

$$\Delta\tau_o = \frac{1}{2}\left(\frac{\Gamma}{\mathbf{b}}\right)^{\frac{3}{2}}\left(\frac{\mathbf{b}\,df}{T}\right)^{\frac{1}{2}}A - \frac{1}{2}\left(\frac{\Gamma}{\mathbf{b}}\right)f \quad (1)$$

where Γ is the anti-phase domain boundary energy (APBE) of the γ′ particles in the {111} plane, and is taken as 0.28 J m^{-2} [22], **b** is the Burgers vector of the edge dislocation in the γ matrix (**b**=1/2[110]a_o, a_o=3.55 Å), d is the particle diameter, f is the volume fraction of the γ′ precipitates, T is the line tension of the dislocation $\left(T=(G\mathbf{b}^2/2)\right)$ and G is the isotropic elastic shear modulus, which is taken as 80 GPa [22]. A is a numerical factor depending on the morphology of the precipitates. For spherical precipitates A=0.72 [23].

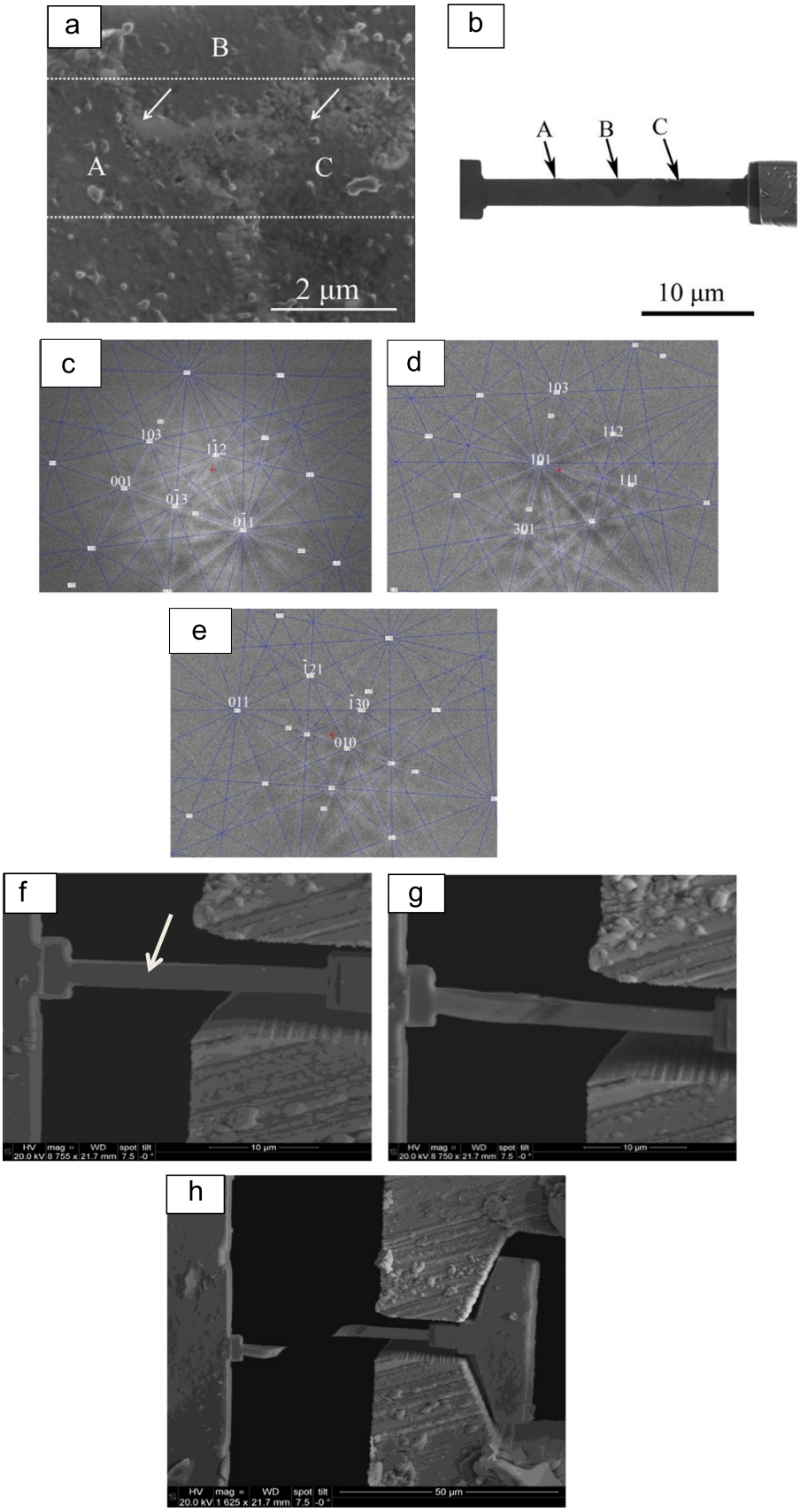

Fig. 5. (a) SEM image of the weld CLZ from where a micro-tensile sample was prepared (inset arrows show the liquation product), (b) micro-tensile sample ($22.89 \times 2.60 \times 3.67\ \mu m^3$) prepared from 'a' (c–e) Kikuchi patterns from grains A, B and C correspondingly. (f and g) microstructures at various strain levels (3.06% and 19.57% correspondingly), illustrating slip formation along the gauge length of the sample. Close observation of 'g' and 'h' with measurements along the gauge length shows that the sample fractured along the liquated grain boundary between grains 'B' and 'C' of 'a'.

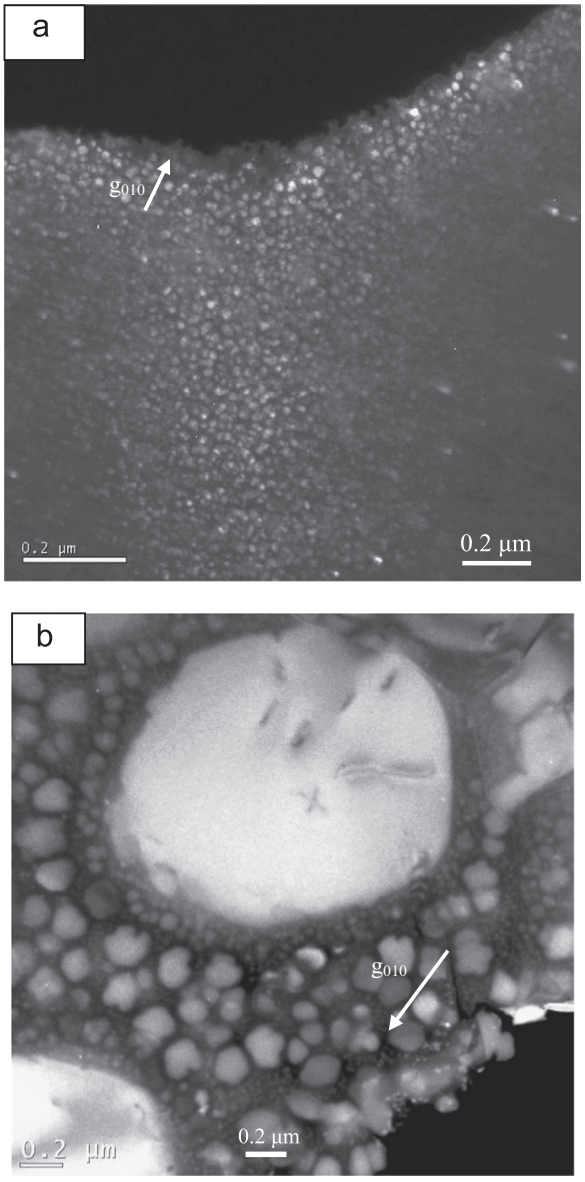

Fig. 6. TEM DF image of (a) re-precipitated tertiary γ′ within 0.3 mm of HAZ of the weld taken with the beam direction ~[103] zone axis and (c) TEM DF image taken with the beam direction ~[101] zone axis, showing the trimodal γ′ precipitates (primary, secondary and tertiary), 4.5 mm away from the bond line (i.e. within the base material).

The strength σ of a precipitation strengthened material has contributions from the solid solution matrix σ_m and the precipitates, σ_p, and follows a linear additivity rule [24] as given in Eq. (2).

$$\sigma_T = \sigma_m + \sigma_p \tag{2}$$

where σ_m is the matrix strength and σ_p is the precipitate strength contribution.

Similarly,

$$\tau_{o(T)} = \tau_{o(\gamma)} + \Delta\tau_{o(\gamma')} \tag{3}$$

where $\tau_{o(T)}$ is the critical resolved shear strength of the alloy, $\Delta\tau_{o(\gamma)}$ is the critical resolved shear strength of the γ matrix and $\tau_{o(\gamma')}$ is the critical resolved shear strength due to the γ′ precipitate.

By taking $f=19\%$ as determined from the weld region and $d=25$ nm for the average diameter of the re-precipitated γ′ within the weld by image J software, we have

$$\Delta\tau_{o(\gamma')} = 222 \text{ MPa}$$

The γ′ precipitates have a tri-modal distribution in the parent material. As a crude estimate, the CRSS in the parent material will be assumed to depend solely on the fraction of tertiary γ′. 8% volume fraction and 25 nm diameter size have been measured for tertiary γ′, which gives

$$\Delta\tau_{o(\gamma')} = 168 \text{ MPa}$$

The difference is 54 MPa, which agrees well with the difference in the CRSS measured and presented in Table 2.

4. Summary

The CRSS of the parent and weld of RR1000 was measured using a micro-tensile test. The results of the micro-tensile tests have shown that the critical resolved shear strength within the weld region is 306 MPa, higher than that of the parent alloy of 255 MPa. The higher strength within the weld region is due to high volume fraction of the re-precipitated tertiary γ′ as confirmed via the formula of Brown. The liquated grain boundary appeared weaker in the tensile test.

Prime novelty statement

Due to the narrow weld zone ($\sim < 1$ mm) and often overmatched strength associated with inertia friction welds, it is difficult to characterize the local mechanical properties of the welded region by using a standard large-scale testpiece geometry. A micro-tensile test method, using focused ion beam machining to make specimens only a few microns in size, for determination of the elastic and plastic properties of candidate materials, is developed. This experimental technique allows the measurement of tensile properties with a much smaller restriction on the volume of material available. The manuscript describes such work carried out on an inertia weld of RR1000, an advanced nickel disc alloy. The study was linked with parallel electron microscopy studies of the effect of precipitate size and distribution, and the effect of some welding features (eutectic liquation products). This provides insight to the hardening and embrittlement of the weld. The results obtained from the current study could also potentially be used for the development and verification of computer models for simulating the mechanical properties of welded joints in RR1000.

It is the first time that micro-tensile experiments have been performed on inertia friction welds in RR1000. This paper should be of interest to a broad readership, including those interested in material characterisation, solid state welding of superalloys, modelling of weld mechanical properties, whether from academia or industry. We declare that this manuscript consists of original, unpublished work which is submitted for the first time to this journal and is not under consideration for publication elsewhere.

Acknowledgement

This work was supported by Rolls-Royce plc and the Engineering and Physical Sciences Research Council under EP/H022309/1 and EP/H500375/1. One of the authors (KMO) also acknowledges a Dorothy Hodgkin Postgraduate Scholarship from the University of Birmingham, United Kingdom.

References

[1] S.M. Spearing, Acta Mater. 48 (2000) 179–196.
[2] M.A. Haque, M.T.A. Saif, Exp. Mech. 43 (2003) 248.
[3] W.N. Sharpe, International Semiconductor Device Research Symposium, 2001, p. 416.

[4] T. Yi, C.J. Kim, Meas. Sci. Technol. 10 (1999) 706.
[5] M. Zupan, K.J. Hemker, Metall. Mater. Trans. A 29 (1998) 65.
[6] D.S. Gianola, S. Van Petegem, M. Legros, S. Brandstetter, H. Van Swygenhoven, K.J. Hemker, Acta Mater. 54 (2006) 2253.
[7] W.N. Sharpe, B. Yuan, R. Vaidyanathan, R.L. Edwards, Microlithography and Metrology in Micromachining II, vol. 2880, 1996, p. 78.
[8] W.N. Sharpe, K.T. Turner, R.L. Edwards, Exp. Mech. 39 (1999) 162.
[9] E.H. Klaassen, K. Petersen, J.M. Noworolski, J. Logan, N.I. Maluf, Sens. Actuator A52 (1996) 132.
[10] D.A. LaVan, W.N. Sharpe, Metall. Mater. Trans. A32 (2001) 913.
[11] K.J. Hemker, W.N. Sharpe, Annu. Rev. Mater. Res. 37 (2007) 93.
[12] D.A. LaVan, W.N. Sharpe, Exp. Mech. 39 (1999) 210.
[13] H. Jin, W. Lu, J. Korellis, Proceedings of the XIth International Congress and Exposition, Orlando, Florida, USA, vol. 41, 2008, p. 1.
[14] M. Preuss, J.W.L. Pang, P.J. Withers, G.J. Baxter, Metall. Mater. Trans. A33 (2002) 3215.
[15] H.Y. Li, Z.W. Huang, S. Bray, G. Baxter, P. Bowen, Mater. Sci. Technol. 23 (2007) 1408–1418.
[16] R.J. Mitchell, M. Preuss, S. Tin, M.C. Hardy, Mater. Sci. Eng. A473 (2008) 158.
[17] M.A. Haque, M.T.A. Saif, Exp. Mech. 42 (2002) 123.
[18] M.A. Haque, M.T.A. Saif, Scr. Mater. 47 (2002) 863.
[19] M.A. Haque, M.T.A. Saif, Exp. Mech. 43 (2003) 248.
[20] L.M. Brown, R.K. Ham, in: A. Kelly, R.B. Nicholson (Eds.), Strengthening Methods in Crystals, Applied Science Publishers Ltd., London, 1971, p. 9.
[21] W. Huther, B. Reppich, Z. Metall. 69 (1978) 628–634.
[22] M.P. Jackson, R.C. Reed, Mater. Sci. Eng. A259 (1999) 85.
[23] B. Reppich, Acta Metall. 30 (1982) 87.
[24] F. Gabrielli, V. Luinc, in: R.C. Gifkins (Ed.), Strength of Metals and Alloys, Pegamon Press, Oxford, 1982, p. 607.